Thermodynamic Study of Water Adsorption in High-Silica Zeolites

Vera Bolis* and Claudia Busco

NIS (Nanostructured Interfaces and Surfaces) Centre of Excellence, INSTM (Materials Science and Technology) National Consortium, UdR Piemonte Orientale, DiSCAFF Università del Piemonte Orientale "A. Avogadro", Via G. Bovio 6, 28100 Novara, Italy

Piero Ugliengo

NIS (Nanostructured Interfaces and Surfaces) Centre of Excellence, INSTM (Materials Science and Technology) National Consortium, UdR Università di Torino, Dipartimento di Chimica IFM Università di Torino, Via P. Giuria 7, 10125 Torino, Italy

Received: February 20, 2006; In Final Form: April 26, 2006

The joint use of microcalorimetric and computational approaches has been adopted to describe H_2O interaction with *cus* Al(III) Lewis and $Si(OH)^+Al^-$ Brønsted acidic sites within H−BEA and H−MFI zeolites (both with ∼6 Al/unit cell). Adsorption data obtained at 303 K were compared to experimental model systems, such as all-silica zeolites, amorphous silica, and silico-alumina, transition alumina. In parallel, ab initio molecular modeling was carried out to mimic, in a cluster approach, Lewis and Brønsted acidic sites, as well as a variety of Si−OH species either with H-bonding interacting (nests and pairs) or isolated. H−BEA and H−MFI water affinity values were found to be almost equivalent, in both quantitative and energetic terms, in that dominated by Al-containing sites population, more than by nanocavity topology or by acidic site nature. Both H-zeolites, saturated with ≈5 Torr of H_2O vapor, bind ∼4 H_2O per Al site, almost one of which is tightly bound and not eliminated by RT pumping-off. A $160 < q^{diff} < 80$ kJ/mol interval was measured for the adsorption up to $1H_2O$/Al. The zero-coverage heat of adsorption ($q_0 \approx 160$ kJ/mol, for both H-zeolites) was assigned to H_2O/Lewis complex formation, which dominates the early stage of the process, in agreement with the ab initio computed H_2O/Lewis sites binding energy. The rather broad q^{diff} interval was interpreted as due to the simultaneous adsorption of H_2O on both structural Brønsted sites and strongly polarized H_2O already adsorbed on Lewis sites. For this latter species, BE = 74 kJ/mol was computed, slightly higher than BE = 65 kJ/mol for H_2O/Brønsted sites interaction, showing that H_2O coordinated on *cus* Al(III) Lewis sites behaves as a structural Brønsted site. The investigated all-silica zeolites have been categorized as hydrophilic in that the measured heat of adsorption ($100 < q^{diff} < 44$ kJ/mol) was larger than the heat of liquefaction of water (44 kJ/mol) in the whole coverage examined. Indeed, polar defects present in the hydrophobic Si−O−Si framework do form relatively stable H_2O adducts. Crystalline versus amorphous aluminosilicate q^{diff} versus n_{ads} plots showed that the measured adsorption heat is lower than expected, due to the extraction work of Al atoms from the amorphous matrix to bring them in interaction with H_2O. On the contrary, such an energy cost is not required for the crystalline material, in which acidic sites are already in place, as imposed by the rigidity of the framework. Modeling results supported the experimental data interpretation.

1. Introduction

Proton-exchanged zeolites are widely used as solid-acid catalysts in several relevant industrial processes.[1−3] Their acidity is related to the presence of $Si(OH)^+Al^-$ species, which are able to adsorb and transform guest molecules by donating protons, i.e., acting as Brønsted acidic sites. A great deal of work has been devoted to the characterization of such sites, and much about their nature and properties is known,[1,4−7] even if their quantitative characterization[2,3,8−13] is not routinely available. The ability to donate protons is not, however, the only feature of acidic zeolites relevant to catalysis. Several experimental studies[9,14,15] have shown that some zeolites are also strong electron acceptors; i.e., they behave as Lewis acids. H−BEA zeolite is a well-known case[16,17] as abundant local defects are localized at the stacking faults between two equally stable crystalline phases. At variance with the detailed knowledge of the Brønsted sites, very little is known about the structure of Lewis sites, and only hypotheses have been suggested in the literature. Some authors associate Lewis acidity in zeolites with framework trigonal Al atoms,[18] whereas other groups have suggested that Lewis sites are made up of extraframework Al(III) species (EFAL) within the pores.[19−23]

A combined experimental and computational approach has been started by us in order to describe the structure of Lewis acidic sites in H-zeolites, as well as to quantify their acidic strength. In particular, the enthalpy changes associated with the adsorption of molecular probes have been determined by microcalorimetry and have been compared to the binding energies obtained through ab initio calculations of the same probes, interacting with model sites simulating Lewis acidic species of modulated strain.[24−26]

* To whom correspondence should be addressed. E-mail: bolis@pharm.unipmn.it. Phone: +39-0321-375-840. Fax: +39-0321-375-821.

10.1021/jp061078q CCC: $33.50
Published on Web 07/06/2006

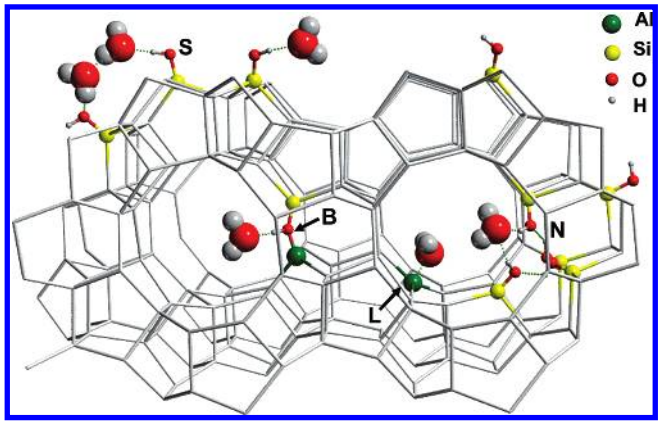

Figure 1. Possible interactions between probe molecules and (acidic) sites located within the nanocavities of a H−MFI zeolite: B = Brønsted acidic site, $Si(OH)^+Al^-$; L = Lewis acidic site, *cus* framework Al-(III); N = Si−OH hydroxyls nest; S = external surface Si−OH. Aspecific interactions (confinement effects) are also operative, owing to dispersion forces generated by nanocavities walls.

Figure 1 illustrates different kinds of possible interactions between H_2O molecules and (acidic) sites located either within the H-zeolite nanocavities or at the external surface, which all contribute to the calorimetrically measured energy of interaction, namely the following: (i) coordination on Lewis acidic sites (L), i.e., on *cus* framework Al(III); (ii) strong H-bonding interaction on Brønsted $Si(OH)^+Al^-$ acidic sites (B); (iii) medium-strength H-bonding interaction on Si−OH species (silanols) forming nests (N) of variable size and geometrical arrangement; (iv) weak H-bonding interaction on isolated silanols (S) exposed at the external surface; (v) aspecific interactions generated by the walls of the nanocavities through dispersion forces, which depend on both structure and size of the pores and molecular probe polarizability (confinement effect).

As far as Brønsted and (possibly present) Lewis acidic sites are concerned, a specific interaction with molecules occurs, which contributes to the measured heat according to the relative population of the sites and the energy of the acid−base interaction, which in turn depends on the relative strength of acidic sites and basic molecular probes. Unfortunately, Lewis acidic species are hardly discriminated calorimetrically from the more abundant Brønsted ones, despite the expected large difference in the acidic strength (larger for L sites). Only if the probe does interact selectively with one of the two sites will they be at least partially discriminated, as was done by us by using CO.[24]

The presence of Si−OH species, which act as weak Brønsted acidic sites, makes the scenario even more complex. Whereas isolated Si−OH species are not expected to compete with B and L acidic sites for the adsorption of molecules via H-bonding, nested Si−OH species do form H-bonding adducts with molecules according to the hydroxylated species geometrical arrangement.[27] The density of nested Si−OH species, which compensate Si vacancies in the framework, is not expected to be high in H-zeolites, but it is very high in all-silica defective zeolites.[28] Only if the (probe) molecule is too large to diffuse into the pores[29−31] will the adsorption be limited to the external surface.

It is well-known that the framework topology plays a role in stabilizing the adducts, but still, the energy related to confinement effect is a minor feature with respect to the specific interactions energy, at least when dealing with probes of moderate size and little polarizability.[7,24,32−34] So, in the case of H-zeolites, both interaction with silanols and confinement effect are expected to contribute very little (at least for small molecular probes) to the calorimetrically measured enthalpy change.

At the beginning of our study, we investigated the acidic properties of H−BEA and H−MFI zeolites through the use of molecular probes selected on the basis of their proton affinity values.[24−26] H_2O has been used as a probe among the others, but its peculiar behavior[25] has forced us to analyze and discuss separately the obtained results. The purpose of the present work is to clarify the water−zeolites interaction mechanism, by analyzing and discussing the various kinds of interactions a H_2O molecule experiences with specific (acidic) sites.

The RT-adsorption of H_2O vapor on two H−BEA and H−MFI zeolites, characterized by a very similar silica-to-alumina ratio and a virtually identical number of Al atoms per unit cell, has been investigated. Adsorption data have also been compared to a number of experimental model systems: (i) two MFI and BEA all-silica zeolites, to investigate the contribution from Si−OH nests and nanocavity confinements effect; (ii) three nonmicroporous materials, to investigate individually the chemistry of both isolated and H-bonded interacting Si−OH groups (all-silica), of $Si(OH)^+Al^-$ and *cus* Al(III) acidic species (silico-alumina), and of *cus* Al(III) species (alumina) on flat surfaces, so avoiding the nanocavity confinements effect.

In parallel, ab initio molecular modeling has been carried out to mimic specific sites of interest, rather than to simulate a given site in a specific zeolite framework. Along this line, Lewis and Brønsted sites, isolated pairs, and nested silanols have been designed in a cluster approach to simulate sites occurring in extended materials. The purpose of the modeling contribution was not to run state of the art simulations, but rather to provide guidelines for the interpretation of experimental energetic data in broad classes of interaction strengths.

2. Experimental Section

2.1. Materials. The interaction of H_2O vapor with the following materials has been investigated.

Microporous Materials. (i) H−MFI is a proton-exchanged MFI zeolite, characterized by a 3D network of straight and sinusoidal channels with accessible pore size of 0.53−0.56 nm, $SiO_2/Al_2O_3 = 7.5$, Al/uc = 6.0 (uc = unit cell).[24,26] (ii) H−BEA is a proton-exchanged BEA zeolite, characterized by three families of interconnected channels with accessible pore size of 0.64−0.76 nm, $SiO_2/Al_2O_3 = 4.9$, Al/uc = 5.9.[24,26] (iii) MFI is Na−Al-free defective MFI−Silicalite, characterized by the same 3D network as H−MFI, and $SiO_2/Al_2O_3 \rightarrow \infty$.[24,26] (iv) BEA is BEA-Silicalite, characterized by the same 3D network as H−BEA, $SiO_2/Al_2O_3 = 255$, Al/uc $\ll 0.1$.[35] It is worth noting that the SiO_2/Al_2O_3 ratio of the two H-zeolites is similar, and that the number of Al atoms per unit cell is the same for the two systems.

All samples were vacuum activated for 2 h at a residual pressure $p \leq 10^{-5}$ Torr (1 Torr = 133.3 Pa), at $T = 673$ K for H−MFI and all-silica zeolites, and at $T = 873$ K for H−BEA. The individual activation temperatures were chosen according to the indications of IR spectroscopy (spectra not reported for the sake of brevity) in order to achieve the maximum dehydration of the surface compatible with the stability of the structure, and to aim for the maximum density of Lewis and Brønsted acidic sites.

Nonmicroporous Materials. The compositional and textural features of the nonmicroporous materials studied for comparison were the following: (i) A300/hy, a high-surface-area amorphous

TABLE 1: Adsorbed Amounts of H_2O on H−BEA, H−MFI, All-Silica BEA and MFI, and Amorphous SA Aluminosilicate, at Water Equilibrium Pressure pH_2O of 0.5 and 5 Torr[a]

	$p = 0.5$ Torr			$p = 5$ Torr		
	mmol/g	H_2O/uc	H_2O/Al	mmol/g	H_2O/uc	H_2O/Al
			H−BEA			
ads I	2.38	9.15	1.5	4.97	19.10	3.2
ads II	1.99	7.65	1.3	4.14	15.92	2.7
ads I − ads II	0.39	1.50	0.2	0.83	3.19	0.5
			H−MFI			
ads I	1.99	11.48	1.9	3.55	20.47	3.4
ads II	1.51	8.71	1.4	2.86	16.50	2.7
ads I − ads II	0.48	2.77	0.5	0.69	3.98	0.7
			BEA			
ads I	0.28	1.08		1.31	5.04	
ads II	0.28	1.08		1.31	5.04	
ads I − ads II						
			MFI			
ads I	0.15	0.86		0.70	4.04	
ads II	0.15	0.86		0.58	3.34	
ads I − ads II				0.12	0.69	
			SA			
ads I	0.56			1.53		
ads II	0.25			0.94		
ads I − ads II	0.31			0.59		

[a] Amounts listed as either mmol/g or molecules per unit cell and per Al atom. Adsorption temperature $T_{ads} = 303$ K.

TABLE 2: Calorimetric Data for H_2O Adsorption on H−BEA, H−MFI, All-Silica BEA and MFI, and Amorphous SA Aluminosilicate, at Water Equilibrium Pressure pH_2O of 0.5 and 5 Torr[a]

	$p = 0.5$ Torr		$p = 5$ Torr	
	Q^{int}	$q_p = [Q^{int}/n_{ads}]_p$	Q^{int}	$q_p = [Q^{int}/n_{ads}]_p$
		H−BEA		
ads I	214.7	90	375.5	76
ads II	146.6	74	287.6	70
ads I − ads II	68.1	175	87.9	106
		H−MFI		
ads I	167.8	84	260.3	73
ads II	108.7	72	197.6	69
ads I − ads II	59.1	123	62.7	91
		BEA		
ads I	17.6	63	73.7	56
ads II	17.6	63	73.7	56
ads I − ads II				
		MFI		
ads I	10	67	48.0	68
ads II	10	67	35.8	61
ads I − ads II			12.2	102
		SA		
ads I	46.6	83	102.2	67
ads II	18.6	74	58.5	62
ads I − ads II	28	90	43.7	74

[a] Q^{int} (J/g), integral heat of adsorption per gram of zeolite, $[q_p]^{mol} = (Q^{int}/n_{ads})_p$ (kJ/mol), integral molar heat of adsorption. Adsorption temperature $T_{ads} = 303$ K.

silica (Aerosil 300 from Degussa, SSA = 296 m^2/g) vacuum-activated at $T = 423$ K ($p \leq 10^{-5}$ Torr, 2 h) in order to eliminate only physisorbed water without affecting H-bonding interacting Si−OH population;[36−38] (ii) A300/dehy, the same amorphous silica but vacuum-activated for 2 h at $T = 923$ K ($p \leq 10^{-5}$ Torr) in order to get rid of all H-bonding interacting Si−OH, and leaving at the surface only isolated Si−OH species, and most likely a few strained siloxane (Si−O−Si) bridges;[36−38] (iii) ALU, a transition alumina (δ-Al_2O_3, Alon-C from Degussa; SSA = 101 m^2/g) vacuum-activated at $T = 1023$ K ($p \leq 10^{-5}$ Torr, 2 h) in order to achieve the maximum surface dehydration/dehydroxylation, so ensuring a high density of Lewis acidic sites, i.e., *cus* Al(III) cations;[29,39−41] (iv) SA: an amorphous analogous of acidic zeolites, i.e., a high-surface-area alumino-silicate (by Strem Chemicals, Inc., $SiO_2/Al_2O_3 = 5.8$, SSA = 311 m^2/g) vacuum-activated at $T = 673$ K ($p \leq 10^{-5}$ Torr, 2 h) again to ensure a maximum density of Lewis and Brønsted acidic sites.[42,43]

H_2O was distilled in vacuo and rendered gas-free by several freeze−pump−thaw cycles.

2.2. Methods. *Adsorption Microcalorimetry.* The heats of adsorption have been measured at 303 K by a heat-flow microcalorimeter (Calvet C80, Setaram) connected to a high vacuum ($p \leq 10^{-5}$ Torr) gas-volumetric glass apparatus, which enables us to determine in the same experiment integral heats evolved (ΔQ^{int}) and adsorbed amounts (Δn_{ads}), for small increments of the adsorptive. A well-established stepwise procedure was followed.[24,26,44] The pressure was monitored by a transducer gauge (Ceramicell 0−100 Torr, Varian). Adsorbed amounts ($n_{ads} = \Sigma\Delta n_{ads}$) and integral heat evolved ($Q^{int} = \Sigma\Delta Q^{int}$) will be reported as a function of the equilibrium pressure (pH_2O), i.e., as volumetric and calorimetric isotherms, respectively. In the microporous systems case, the adsorbed amounts will be reported either as millimoles of H_2O per gram of zeolite (n_{ads}, mmol/g, see volumetric isotherms and Table 1), or as H_2O molecules per unit cell (uc) (see Table 1) in order to compare from a structural point of view the affinity toward H_2O. For H-zeolites, the number of H_2O molecules adsorbed per Al atom will also be reported. Conversely, for nonmicroporous materials, n_{ads} will be reported as micromoles per square meter of the surface (see volumetric isotherms). For SA, the adsorbed amounts will be reported also as millimoles per gram (see Table 1). Integral heats will be reported per gram of zeolite (Q^{int}, J/g) or per square meter of the surface (Q^{int}, J/m^2), as shown in the calorimetric isotherms, or in kilojoules per mole as integral molar heats of adsorption. This latter quantity is defined as $[q^{mol}]_p = (Q^{int}/n_{ads})_p$ and is the integral heat of adsorption normalized against the adsorbed amount at any chosen equilibrium pressure (see Table 2). The $[q^{mol}]_p$ heats of adsorption are intrinsically average values, as they refer to the thermal response of the surface as a whole, from the beginning of the process up to the equilibrium pressure at which they have been measured. The reversibility/irreversibility upon RT-evacuation of first run adsorbed phase (ads I) was checked by performing a second run (ads II) after outgassing the sample overnight ($p \leq 10^{-5}$ Torr). By subtracting the ads II curve from that of ads I, the adsorbed fraction not removed by evacuation was evaluated. The ads II component will be hereafter referred to as the reversible adsorbed phase, whereas the (ads I − ads II) component will be referred to as the irreversible one (in the adopted conditions). A third run of adsorption (ads III) has been performed in all cases and turned out to be coincident with ads II. It will not be reported for the sake of brevity. (The adsorption measurements have been performed at least twice on a virgin portion of the same batch of the materials, activated in the same conditions, to check the reproducibility of the experiments.)

The equilibrium quantitative and calorimetric data have been also processed in order to obtain the differential heats of adsorption, i.e., the enthalpy change ($q^{diff} = -\Delta_{ads}H$) associated with the process. Differential heats of adsorption are defined as the derivative ($q^{diff} = \delta Q^{int}/\delta n_{ads}$) of the $Q^{int} = f(n_{ads})$ function, which best fits the Q^{int} versus n_{ads} equilibrium data (plots not reported for the sake of brevity).[43−47] An alternative route for

evaluating q^{diff} has, however, been followed in the present paper, as has already been described.[13,48−53] The q^{diff} versus n_{ads} curves, shown in the Results and Discussion section, are the exponential functions which best fit the experimental points obtained by taking the middle points of the partial molar heats ($\Delta Q^{int}/\Delta n_{ads}$, kJ/mol) versus n_{ads} histogram. [The ($\Delta Q^{int}/\Delta n_{ads}$, kJ/mol) quantity corresponds to the adsorbed-amount-normalized heat evolved during the adsorption of the individual doses (prepared as small as possible) according to the stepwise procedure.]

It is worth noting that the limit for Δn_{ads} approaching zero is the true differential heat:

$$\lim_{\Delta n_{ads} \to 0} (\Delta Q^{int}/\Delta n_{ads}) = q^{diff} \quad (1)$$

The q^{diff} values will be reported also as a function of H_2O equilibrium pressure.[49] Whereas the integral molar heats of adsorption $[q^{mol}]_p$ are intrinsically average values, differential heats of adsorption represent a reasonable measure of the energy of interaction of a probe molecule with individual sites, at any adsorbate coverage. So, q^{diff} versus n_{ads} plots give a detailed description of the surface heterogeneity. In particular, q^{diff} versus n_{ads} plots extrapolated to vanishing coverage [$(q_0) = -\Delta_{ads}H_0$] give the enthalpy changes associated with the adsorption on the most energetic sites, active in the earliest stages of the process. These quantities are fruitfully compared with the binding energies (BEs) obtained through ab initio calculations, as will be illustrated below.

Molecular Modeling. All calculations have been run at ab initio level using the B3-LYP/6-31+G(d,p) model chemistry on selected molecular clusters, modeling the different sites. To maximize structural coherence across the different simulated sites (Lewis, Brønsted, and silanols), all clusters have been cut out from the edingtonite structure. Edingtonite is a microporous zeolite and has been previously adopted by some of us to mimic the hydroxylated surface of amorphous silica.[54,55] In this work, it was proven that clusters properly cut out from the periodic crystal successfully represent the infinite system's physicochemical features.

For the Lewis site, owing to the large uncertainty of the local structure around the Al atom, two topological different clusters (LS and LC structures) have been adopted, as shown in Figure 2. LS model (the only one not belonging to the edingtonite framework) has been previously adopted by us,[24,25] to mimic highly strained coordinatively unsaturated Al(III) moieties. Conversely, the new LC cluster structure simulates the surface Al(III) species lowering their coordinative unsaturation by coordinating to an additional nearby framework oxygen.

Brønsted $Si(OH)^+Al^-$ sites, H-bonding interacting (nests and pairs), and isolated Si−OH species have been modeled by clusters hereafter referred to as B, N, P, and S structures, respectively, as shown in Figure 2. Structures envisaging H_2O adsorbed upon the sites are shown in Figure 3.

The structure of all clusters, either free or interacting with water, have been fully optimized at B3LYP/6-31+G(d,p). All water binding energies (BEs) have been corrected for the basis set superposition error, using the standard Boys−Bernardi counterpoise method.[56]

3. Results and Discussion

3.1. Microporous Systems: H-Zeolites. In Figure 4, data for H_2O adsorbed on H−MFI and H−BEA are reported in comparison with those obtained for MFI and BEA all-silica zeolites. Volumetric isotherms are shown in part a, and calorimetric isotherms in part b. The following can be noted:

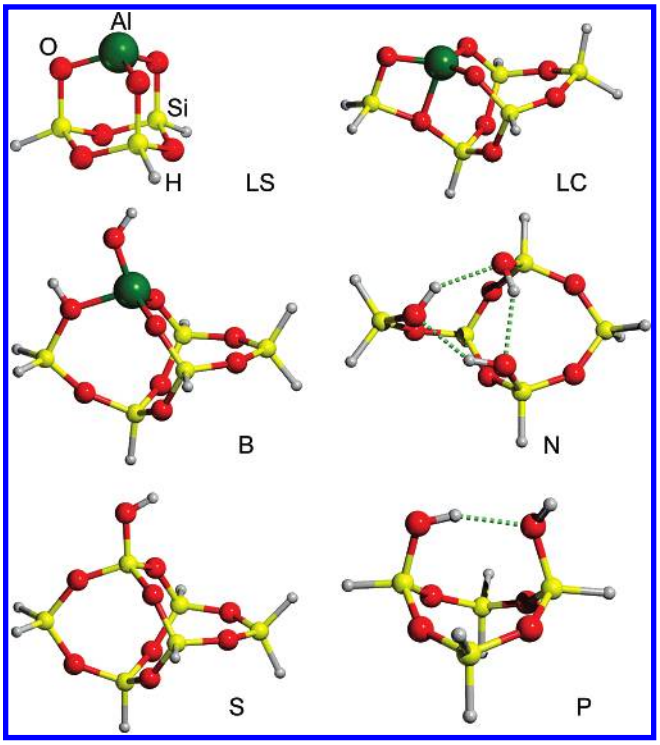

Figure 2. B3LYP/6-31+G(d,p) optimized clusters adopted to mimic the strained Lewis site (LS), the extra-coordinated Lewis site (LC), the Brønsted site (B), the hydroxyl nest site (N), the isolated silanol (S), and the H-bonding interacting SiOH pair (P). Hydrogen bonds as dotted lines.

(i) H-zeolites exhibit, as expected, a much higher affinity toward H_2O than the Al-free systems, but the affinity toward H_2O of the latter is not so small and indicates that hydrophilic sites are developed in zeolites even in the absence of framework Al. (ii) The H_2O/H-zeolites interaction is only partially reversible upon outgassing at room temperature, as witnessed by the noncoincidence of ads I and ads II curves. So, a fraction of the Lewis and/or Brønsted site complexes are stable upon RT-evacuation. (iii) The shapes of the volumetric/calorimetric isotherms of the two homologous (proton-exchanged and all-silica) BEA and MFI zeolites are very similar. In particular, as far as pH_2O increases, both n_{ads} and Q^{int} increase more appreciably for BEA framework, characterized by cavities larger than MFI (0.64−0.76 nm vs 0.53−0.56 nm, respectively).

Adsorption data at low (pH_2O = 0.5 Torr) and high (pH_2O = 5 Torr) equilibrium pressure are reported for the four investigated systems in Table 1 (adsorbed amounts) and Table 2 (integral heats of adsorption). From inspection of Tables 1 and 2, the following is noticed: (i) The number of H_2O molecules adsorbed per unit cell is similar for H−BEA and H−MFI, despite their different structure and distribution of L and B sites. Further, as the number of Al atoms present in the two H-zeolites unit cells is almost the same, it turns out that the number of H_2O molecules per Al atom is also very close. This holds at both low and high pH_2O: 1.5 vs 1.9 and 3.2 vs 3.4 H_2O/Al atom for H−BEA vs H−MFI at pH_2O = 0.5 and 5 Torr, respectively. (ii) Also, the average energy of H_2O-acidic sites interaction is similar for the two H-zeolites, as indicated by the $[q^{mol}]_p$ values, both at low (90 vs 84 kJ/mol) and high (76 vs 73 kJ/mol) pH_2O, for H−BEA versus H−MFI. (iii) As for the reversible phase (ads II), the similarities of the two H-zeolites are still more evident, in both quantitative and calorimetric terms. In both cases, ads II curve lies well below that of ads I, and corresponds to ∼80% of the total adsorbed phase. The $[q^{mol}]_p$ value for the two H-zeolites is very similar, close to ∼70

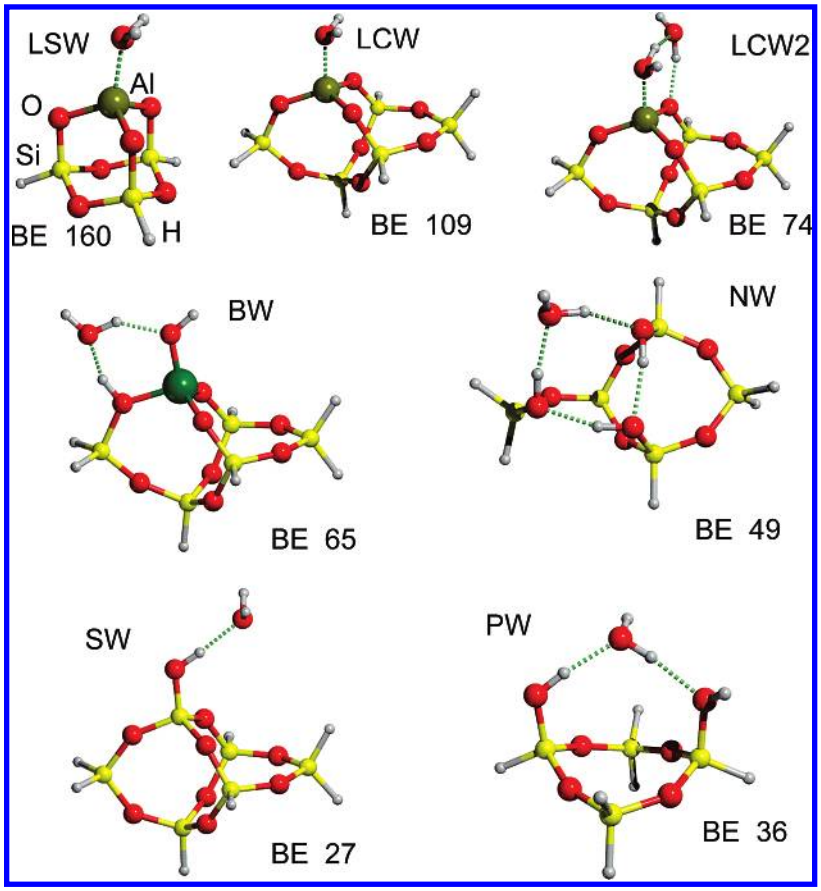

Figure 3. B3LYP/6-31+G(d,p) optimized structures of the clusters interacting with H_2O molecule. Binding energies (BEs) corrected for the basis set superposition error in kilojoules per mole. For LCW2, the BE refers to the second H_2O molecule interacting with the LCW cluster. Atomic symbols are reported in Figure 1. Hydrogen bonds and bonds between Al and the oxygen atom of the adsorbed water shown as dotted lines.

kJ/mol, at both low and high pH_2O. (iv) The irreversible component, estimated by the (ads I − ads II) difference, turns out to be ∼20% of the total adsorption, for both H-zeolites. The $[q^{mol}]_p$ value (in both cases) either does exceed 100 kJ/mol (low pH_2O) or is close to 100 kJ/mol (high pH_2O).

3.2. Microporous Systems: All-Silica Zeolites. Opposite of that of the H-zeolites, H_2O adsorption on all-silica systems is essentially reversible upon RT-evacuation: only weakly bonded species are formed in the Al-free framework, as indicated by the closeness of the ads I and ads II curves.

From the inspection of Table 1, it is seen that the number of H_2O molecules adsorbed per unit cell is quite low with respect to H-zeolites, at both low and high pH_2O, as expected. At p = 0.5 Torr, the uptake is ∼1 H_2O/uc on all-silica against ∼10 H_2O/uc on H-zeolites, whereas at p = 5 Torr it is ∼5 H_2O/uc against ∼20 H_2O/uc for all-silica and H-zeolites, respectively. However, despite the absence of specific Lewis and Brønsted acidic sites, the heats of adsorption indicate a substantial nonhydrophobic character of the all-silica zeolites investigated, in that the $[q^{mol}]_p$ value is larger than q_{LIQ} = 44 kJ/mol (the latent heat of liquefaction of water) in the whole coverage examined. This means that either defective sites such as Si−OH nests (MFI−Silicalite) or Na−Al impurities and Si−OH nests (BEA-Silicalite) make the all-silica microporous systems capable of specifically interacting with water. Indeed, for MFI−Silicalite it has been demonstrated that defective materials do possess mild Brønsted acidic character imparting some catalytic relevance in the Beckman rearrangement of cyclohexanone oxime into caprolactam.[28,57]

In defective MFI−Silicalite, the onset of irreversible phenomena has been observed, as witnessed by the high-pressure noncoincidence of ads I and ads II isotherms (both volumetric and calorimetric, see Figure 4). The high-pressure $[q^{mol}]_p$ value for the irreversible (ads I − ads II) component is as high as 100 kJ/mol, which is compatible with a dissociative process on strained Si−O−Si bridges (vide infra dehydroxylated amorphous silica). This datum suggests that some Si−O−Si bridges in the Al-free structure are strained and react (at high pH_2O) with H_2O adsorbed on Si−OH nests.

3.3. Differential Heats of Adsorption (Proton-Exchanged and All-Silica Zeolites). In addition to the quantitative molar information arising from the isotherms, more details on the energetics of the interaction are given by the differential heats of adsorption, which are reported in Figure 5, either as a function of coverage (part a) or as a function of the H_2O equilibrium pressure (part b). The exponential function, which best fits the experimental q^{diff} versus n_{ads} values shown in part a of the figure, turns out to be the same for the two H-zeolites, despite their supposedly different Lewis and Brønsted site distribution. This fact does confirm that also at the molecular level the affinity toward H_2O of the two acidic zeolites is very similar, and is a strong indication, contrary to that indicated by data in our previous work,[24] that the H−BEA and H−MFI acidic site distribution (L and B in nature) is not so different, at least as far as H_2O is used as the molecular probe.

The first run heat of adsorption decreases from an initial high value ($q_0 \approx$ 160 kJ/mol) down to ∼80 kJ/mol, at a coverage equivalent to ∼1 H_2O molecule per Al atom (as average). Afterward, at a coverage equivalent to ∼2 H_2O/Al, q^{diff} reaches a value of ∼60 kJ/mol and remains constant up to the highest coverage investigated in the present work (∼4 H_2O/Al).

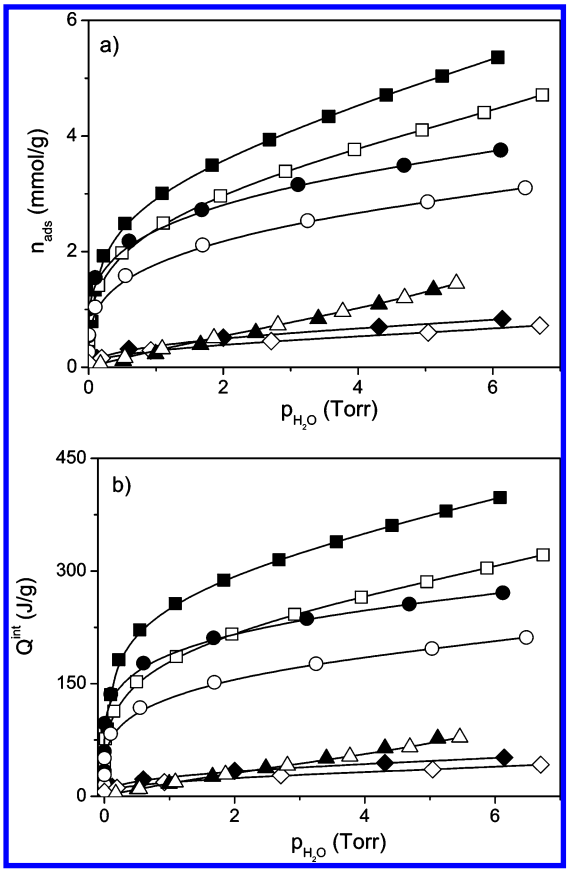

Figure 4. (a) Volumetric isotherms (adsorbed amounts vs equilibrium pressure) and (b) calorimetric isotherms (integral heat evolved vs equilibrium pressure) of H_2O adsorbed at $T = 303$ K on H−MFI (●, ○), H−BEA (■, □), all-silica MFI (◆, ◇), all-silica BEA (▲, △) zeolites. Solid symbols correspond to the first run; open symbols correspond to the second run.

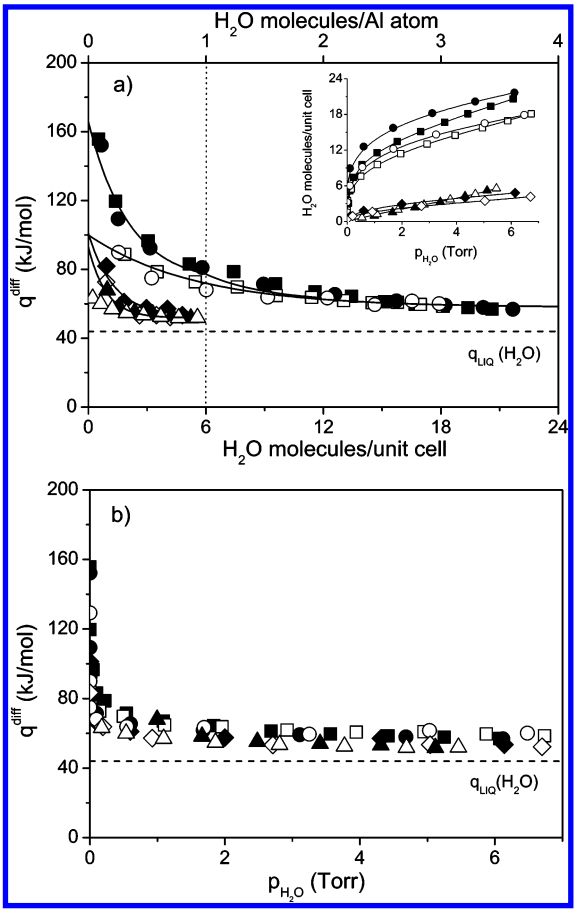

Figure 5. Differential heats of adsorption of H_2O at $T = 303$ K on H−MFI (●, ○), H−BEA (■, □), all-silica MFI (◆, ◇), all-silica BEA (▲, △) zeolites. (a) q^{diff} vs coverage. (b) q^{diff} vs H_2O equilibrium pressure. Solid symbols correspond to the first run; open symbols correspond to the second run. Inset of part a indicates volumetric isotherms reported as H_2O molecules/uc vs equilibrium pressure.

The low-coverage heat values ($q^{diff} > 100$ kJ/mol) are compatible with the energy of coordination of H_2O on L acidic sites involving highly strained *cus* Al(III) sites, as modeled by the LSW cluster reported in Figure 3 (vide infra its discussion). This datum confirms the presence of L acidic sites in both investigated H−BEA and H−MFI zeolites. In fact, the presence of Lewis acidic species is likely unavoidable in MFI microporous systems. It is indeed recognized that a variable amount of Al defects is always present in such materials and that H-zeolites showing the sole Brønsted acidity are very rare.[42,58,59] The presence of a small amount of L acidic sites in our H−MFI specimen was already put in evidence by us through the adsorption of N_2 and CO,[24] but the close similarity of the two q^{diff} versus n_{ads} plots in the whole H_2O coverage interval examined is somehow surprising, in that at least in the early stage of the adsorption process we would have expected the H−MFI curve to lie below the H−BEA one. This was expected because (i) from N_2 and CO adsorption data H−MFI was thought to be less rich in Lewis sites than H−BEA, and (ii) our modeling results show (vide infra) that the acidic strength of L and B sites is dramatically different.

To simulate the very low coverage, quantum mechanical calculations have been carried out on LS and LC models of Lewis sites (Figure 2) interacting with one H_2O molecule (Figure 3, LSW and LCW structures). The LS model, in virtue of the geometrical strain around the Al(III) atom, sports the largest affinity toward H_2O, with a binding energy (BE) of about 160 kJ/mol, close to the zero-coverage heat of adsorption measured for both H-zeolites (see the extrapolated q_0 value in Figure 5). A smaller binding energy (BE = 109 kJ/mol) has been computed for the LC model. This was expected, in that the Al(III) moiety is almost tetrahedrally coordinated in a free LC cluster, and a large fraction of the interaction energy is lost to rearrange the local coordination around the Al atom. This is clearly shown in the LCW structure (Figure 3) in which pristine coordination of Al(III) with framework oxygen is lost, in favor of a stronger interaction with the adsorbed H_2O oxygen atom. By computing LCW binding energy without including the geometrical rearrangement cost (i.e., keeping LC in the geometry assumed in the complex), a BE = 143 kJ/mol is arrived at, showing that ca. 34 kJ/mol is due to geometrical relaxation. By comparing this BE = 143 kJ/mol value with BE = 160 kJ/mol computed for the LS cluster, it turns out that ∼20 kJ/mol upon 160 kJ/mol are due to the geometrical strain around Al(III) atom, which is imposed by the LS cluster topology. Such results show that local topology around Al(III) and framework flexibility may impart a significantly different Lewis acidic strength to coordinatively unsaturated Al(III) atoms. Further discussion on this important point will be addressed in the section devoted to the crystalline-microporous versus amorphous alumino-silicate materials comparison (vide infra).

Adsorption of H_2O on a Brønsted site (structure B, Figure 2) as modeled by the BW structure (see Figure 3) shows H_2O acting both as a H-bond acceptor of the Brønsted acidic proton, and as a H-bond donor toward a framework oxygen (here modeled by a terminal OH group).[60] Even if the adopted model is rather minimal, the computed BE = 65 kJ/mol is close to the

best quantum mechanical calculation results carried out by Tuma and Sauer on H_2O adsorbed on crystalline H−SSZ13.[61] They computed, in a periodic approach, a BE = 70 kJ/mol using a PBE functional and a plane wave basis set coupled with a local MP2 correction to include dispersive contribution.

By comparing modeling results with heat of adsorption values reported to date, theoretical and experimental data are in reasonable agreement as far as H_2O/Brønsted site interaction is concerned, even if a straightforward comparison cannot be made because the experimental heat data reported are rather uncertain and cover a wide range of values: 34−51,[62] 51−85,[60] 40−52,[63] 90 ± 10,[64] or 60−100 kJ/mol.[65] Conversely, no comparison can be made between modeling and experimental data concerning H_2O adsorbed on Lewis sites located within zeolites nanocavities, in that to the best of our knowledge no heat of adsorption data for such species have been discussed in the literature.

The BE values obtained for the various model sites clearly indicate that H_2O molecules interact much less strongly with B sites (65 kJ/mol) than with L sites (160−109 kJ/mol range), whatever the local coordination of Al(III) atom is in the latter. So, we are forced to interpret the coincidence of the two q^{diff} versus n_{ads} plots as due to at least two concomitant effects: (i) Contrary to molecular probes as soft as N_2 and CO, which are able to interact at RT only with the strongest L sites, H_2O is able to detect also the weaker Lewis acidic sites not revealed by soft probes. It is so inferred that the L and B sites distribution is very similar in both H−BEA and H−MFI zeolites (it is worth noting that we previously observed similar behavior by using NH_3 an CH_3CN molecular probes[26]). (ii) The filling of the sites upon increasing pH_2O does not follow an ordered path (which should involve first the adsorption on the strongest sites, mainly L, and then on the weak sites, mainly B) but occurs simultaneously on both kind of sites because B sites are by far more abundant than L sites. This results in a very complicated scenario, in that when different kind of sites are simultaneously involved, the calorimetrically measured heats are the average among different contributions.

So, from the q^{diff} versus n_{ads} plots reported in Figure 5a, it is hard to make a straightforward assignment of the energy related to H_2O adsorption onto individual L and B sites. The $160 < q^{diff} < 80$ kJ/mol heats interval can be straightforwardly assigned only to the progressive binding of H_2O on Al-containing sites, with no chance to definitely single out H_2O/L and H_2O/B interaction. Further, the $160 < q^{diff} < 80$ kJ/mol interval is quite broad and indicates a highly heterogeneous distribution of surface Al-containing sites, compatible with a variety of structurally and/or chemically different sites. Indeed, in the present work modeling results have shown that H_2O coordinated to Al(III) sites originates Lewis acid−base complexes (LCW structure, Figure 3), in which the H-bond donor capability of the adsorbed H_2O molecule is strongly enhanced by the electron transfer and polarization toward the Al(III) atom of the LC cluster. This causes the H_2O molecule adsorbed on a L site to behave similarly to a structural Brønsted site, in that it engages a strong H-bonding interaction with a second H_2O molecule (LCW2 structure in Figure 3). The BE of this complex is 74 kJ/mol, which is even larger than that computed in the present work for the structural B site (BE = 65 kJ/mol, structure BW of Figure 3). This behavior is general, and it applies also to the LS site (data not reported for the sake of brevity).

So, as far as H_2O is adsorbed on strong L sites, the acidity of the latter is not completely quenched, but just the opposite: the acidic strength of newly created sites is still as large as that of structural B sites. In fact, the acidic strength of the sites is expected to increase in the same order as the BE of the various H_2O/site complexes described above: LCW (BE = 160−140 kJ/mol) ≫ LCW2 (BE = 74 kJ/mol) > BW (BE = 65 kJ/mol). In the very early stage of the process, the adsorption on strong L sites is expected to dominate the interaction because of enthalpic reasons, and so the q_0 values can be reasonably assigned to the coordination of H_2O on such sites. Afterward, as far as strongest L sites have been saturated, a variety of sites such as the weaker L sites, LCW sites (H_2O coordinated onto strong L sites), and B sites do participate in forming H_2O complexes. So, a precise heat value for H_2O adsorption on B sites cannot be assigned straightforwardly, in that experimental heat values ($160 < q^{diff} < 80$ kJ/mol) reported for the first-shell coordinated H_2O are indeed comprehensive, in both H-zeolites, of the heat of formation of both H_2O/L and H_2O/B complexes. This fact is most likely one of the reasons why such a broad range of experimental heat values is reported in the literature (vide supra). Despite such a large uncertainty, we suggest a 80−100 kJ/mol interval as the most appropriate for the H_2O/B complexes. Such an interval corresponds indeed to the heat measured for the filling of the second part of the first shell sites, when most likely adsorption on strong L sites is no longer predominant. This assignment is in reasonably good agreement with computational data, both reported in the literature and obtained in the present work. Furthermore, it is also in good agreement with both Olson[65] and Lee and Gorte's[64] experimental H_2O adsorption data: the former reported an isosteric heat of adsorption on H−MFI exceeding 105 kJ/mol (at vanishing coverage), and the latter a calorimetrically measured heat of adsorption of 90 ± 10 kJ/mol.

Once the first shell is completed (or most likely before, if we consider that the H_2O/L complexes are as strong as structural B sites), a second shell is edificated on the top of the first one. This process involves an enthalpy change in the $80 < q^{diff} < 60$ kJ/mol interval (see in Figure 5a the q^{diff} correspondent to the adsorption of a second H_2O molecule per Al). It is worth noting that q^{diff} is still high if compared to $q_{LIQ} = 44$ kJ/mol. This confirms what was suggested from our modeling results, that H_2O species coordinated on Lewis Al(III) sites are strongly polarized and possess an acidic strength comparable to that of structural Brønsted acidic sites. After the completion of the second shell a third one is formed, with an almost constant $q^{diff} \approx 60$ kJ/mol in both H-zeolites, still well above 44 kJ/mol (up to a coverage of ∼4H_2O/Al atom). Olson et al. previously reported that H_2O heat of adsorption on H−MFI approaches 44 kJ/mol only at very high coverage (∼8 H_2O/Al).[65]

By the inspection of ads II reversible curves, still the q^{diff} versus n_{ads} experimental points for the two H-zeolites are interpolated by the same curve, from $q_0 \approx 100$ kJ/mol down to ∼60 kJ/mol. In both cases, H_2O species not removed by overnight evacuation belong to the tightly bound first-shell fraction ($q^{diff} > 100$ kJ/mol). At higher coverage (after the first shell is completed) ads I and ads II q^{diff} curves merge at the same constant value (∼60 kJ/mol).

As far as all-silica zeolites are concerned, the q^{diff} values are obviously much lower than for the protonic form of the materials but are larger than 44 kJ/mol in the whole interval examined (see Figure 5a). In particular, the ads I q_0 is around 100 kJ/mol for both zeolites, and drops very fast down to an almost constant value, slightly higher than 44 kJ/mol. This confirms also at the molecular level that the investigated all-silica zeolites are definitely hydrophilic.

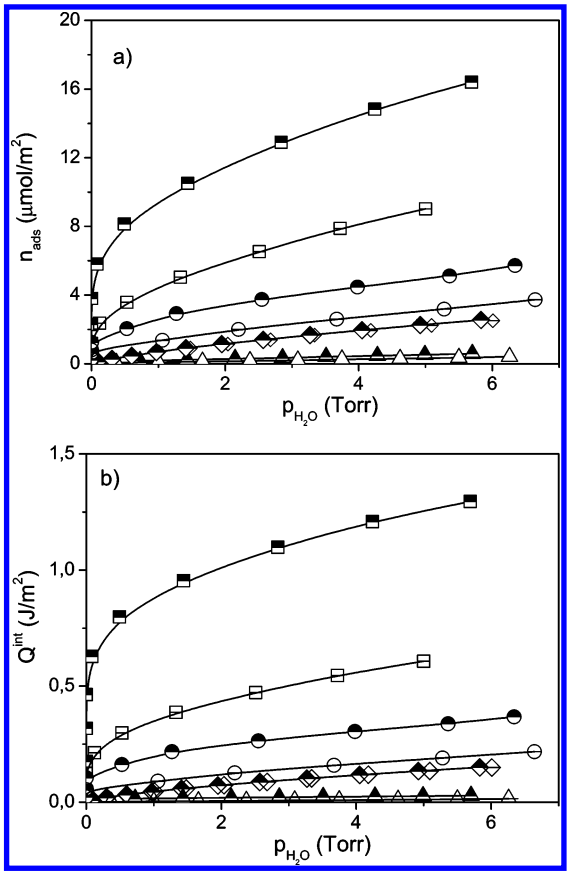

Figure 6. (a) Volumetric isotherms (adsorbed amounts vs equilibrium pressure) and (b) calorimetric isotherms (integral heat evolved vs equilibrium pressure) of H_2O adsorbed at $T = 303$ K on A300/hy (half-filled diamond, open diamond with bisecting line); A300/dehy (half-filled triangle, open triangle with bisecting line); SA (half-filled circle, open circle with bisecting line); ALU (half-filled box, open box with bisecting line). Solid symbols corespond to the first run; open symbols correspond to the second run.

Results from molecular modeling reveal that when the nest structure N (see Figure 2), envisaging three mutually H-bonding interacting Si−OH in order to simulate the Al-free zeolites defects, is put in contact with H_2O (NW model, Figure 3), the computed energy is BE = 49 kJ/mol, which is not dramatically distant from that computed for B sites (BE = 65 kJ/mol, BW model in Figure 3). This datum accounts for the relatively high values of the experimental q_0 for Al-free zeolites.

In Figure 5b, q^{diff} is reported as a function of pH_2O. It is clearly evident that differences between protonic and all-silica zeolites are limited to the early stages of the process, which occur without an appreciable equilibrium pressure and involve specific acidic sites through the formation of either coordinated or strongly H-bonded species. Afterward, the interplay of weak H-bonding (second-to-fourth H_2O adsorbed shell in proton-exchanged, and Si−OH nests in all-silica zeolites) and dispersion-forces interactions (confinement effect) are very similar for all investigated systems.

3.4. Nonmicroporous Systems. In Figure 6, volumetric (part a) and calorimetric (part b) isotherms for H_2O adsorption on the nonmicroporous materials are reported.

Amorphous silica affinity toward H_2O is strongly dependent upon the pretreatment conditions, which govern the actual abundance of the hydrophilic H-bonding interacting Si−OH species.[36−38,49,50,52] For the low-T activated Aerosil, the interaction is fully reversible and at least fourfold larger than for the high-T activated sample: at $p = 5$ Torr the ads I H_2O uptake

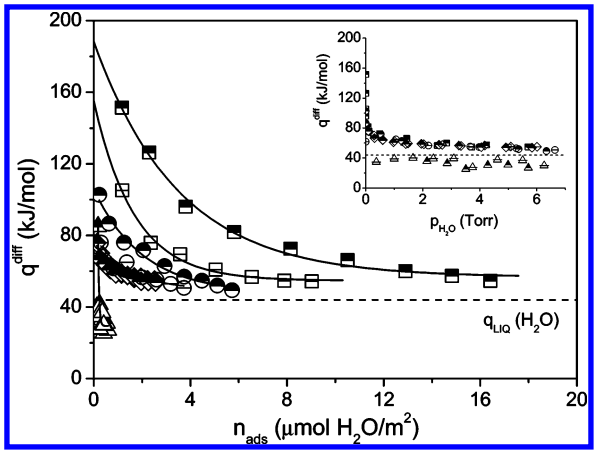

Figure 7. Differential heats of adsorption q^{diff} vs coverage of H_2O at $T = 303$ K on A300/hy (half-filled diamond, open diamond with bisecting line); A300/dehy (half-filled triangle, open triangle with bisecting line); SA (half-filled circle, open circle with bisecting line); ALU (half-filled box, open box with bisecting line). Inset: q^{diff} vs H_2O equilibrium pressure. Solid symbols correspond to the first run; open symbols correspond to the second run.

is 2.16 for A300/hy versus 0.53 μmol/m^2 for A300/dehy. For A300/dehy, the interaction was partially irreversible (ads I and ads II curves are not coincident). The partial irreversibility of the adsorbed phase upon RT-evacuation is likely due to the reaction of H_2O with Si−O−Si bridges, which have been strained as a consequence of the high-T activation.[37] The affinity toward H_2O of dehydroxylated alumina (ionic oxide) is significantly larger than that of the fully hydroxylated silica (covalent oxide): at $p = 5$ Torr the ads I H_2O uptake is 15.61 for ALU versus 2.16 μmol/m^2 for A300/hy. This is not surprising in that ALU exposes at the surface abundant sites capable of strongly interacting with H_2O, either through a strong coordination (*cus* Al^{3+}) or through a dissociative mechanism (*cus* $Al^{3+}-O^{2-}$ pairs).[39,49] The onset of a specific reactivity in ALU is witnessed also by the large irreversibility of the process. SA silico−alumina catalyst exhibits an intermediate behavior between silica and alumina samples. SA affinity toward H_2O is threefold lower than that of the Lewis-acidic ALU (4.90 for SA vs 15.61 μmol/m^2 for ALU, at $p = 5$ Torr), but similar to the latter, the adsorption is largely irreversible.

In Figure 7, q^{diff} versus H_2O coverage plot is reported for the investigated nonmicroporous systems. In the inset of the figure, the q^{diff} versus pH_2O plot is also shown. In all cases examined (with the remarkable exception of A300/dehy), q^{diff} decreases exponentially versus increasing coverage, as is typical of heterogeneous surfaces. Conversely, A300/dehy develops a heat of adsorption virtually constant in the whole pH_2O interval examined and lower than $q_{LIQ} = 44$ kJ/mol, as typical of a hydrophobic surface.[50,52,66,67] Indeed, the adsorption of H_2O is very weak and occurs on isolated silanols, the only residual hydroxylated species either present at the high-T activated SiO_2 surface,[36−38,49,50,52] or exposed at the external surface of zeolites.[59] Isolated Si−OH terminations are able to bind H_2O through only one H-bonding, with a measured heat of adsorption as low as 25−35 kJ/mol.[52,67] Molecular modeling using the cage cluster S (see Figure 2) gives a H_2O BE = 27 kJ/mol (SW structure, Figure 3), not very far from previous results for the minimal H_3SiOH cluster.[68−70]

The very initial H_2O heat of adsorption on A300/dehy (first run) is dramatically high ($q_0 > 120$ kJ/mol) if compared with the very low values ($q^{diff} < 44$ kJ/mol) at high coverage. This result, together with the onset of some irreversibility (at high pH_2O), is a strong indication that a few strained Si−O−Si

bridges (originated by high-T activation) are opened upon interaction with H_2O. This process implies a dissociative adsorption leading to the formation of new Si−OH groups, which is well-known in the literature.[37] This confirms the assignment of the irreversible adsorption $[q^{mol}]_p$ as high as 102 kJ/mol (see Table 2) to the opening of strained siloxane bonds on MFI−Silicalite.

Opposite to dehydroxylated silica, q^{diff} on the hydroxylated specimen (A300/hy) is larger than 44 kJ/mol in the whole interval examined. The surface hydrophilicity is due to the presence of abundant H-bonding interacting Si−OH groups, forming chains of variable length.[36−38,49,50] By comparing Figures 5 and 7, it is inferred (at least in energetic terms) that the affinity toward H_2O of the hydroxylated nonporous Aerosil compares with that of the microporous all-silica zeolite. Comparison with molecular modeling results is, however, not straightforward and deserves a comment. The simple P cluster (see Figure 2), adopted to mimic a pair of H-bonding interacting Si−OH species, gives a H_2O BE = 36 kJ/mol (structure PW, Figure 3), which is some 25% higher than that of H_2O adsorbed on isolated Si−OH (structure SW, Figure 3). This value is, however, smaller than BE = 49 kJ/mol computed for H_2O adsorbed on a Si−OH nest (model NW, Figure 3), meant to mimic the Si vacancies defects in all-silica zeolites. It is worth stressing that the PW model only accounts for pairs of H-bonding interacting Si−OH, while longer chains or even rings are possibly present at the amorphous silica surface. For these, larger H_2O BE values are expected from calculations, because of enhanced H-bonding cooperative effects induced by the Si−OH chains length.[27,71]

The initial heat of adsorption for A300/hy ($q_0 \approx 80$ kJ/mol) is lower than for SA ($q_0 \approx 110$ kJ/mol) and confirms that the presence of Al species in a silica matrix develops a specific reactivity toward H_2O, even if a clear understanding of the water/aluminosilicate surface interaction is not yet available. For the ionic dehydroxylated ALU, q_0 is much higher (∼180 kJ/mol) than for the covalent de-hydroxylated SA, indicating that the Al species in this latter are less available for the interaction than the ALU *cus* Al^{3+} cations, which are next to basic *cus* O^{2-} species. This is likely due to a more severe surface reconstruction occurring in the covalent amorphous SA.

Beside the high q^{diff}, the specific reactivity of the Al-containing systems is also witnessed by the onset of irreversible phenomena, not observed for the fully reversible H_2O−A300/hy interaction. Still, it should be mentioned that the percentages of the irreversible components are identical for SA and ALU (around 40% of the total adsorption).

Regarding the surface coverage increases, the heat values (with the already discussed A300/dehy exception) decrease approaching a constant value, close to the latent heat of liquefaction of water, for silica, alumina, and silico−alumina ($q^{diff} \approx 50$ kJ/mol). This datum indicates that the edification of liquidlike water multilayers seems to be favored by the flatness of the surface.

The q_0 value measured for H_2O adsorbed on Lewis acidic ALU (≈180 kJ/mol) is an indication that the high q_0 value for H-zeolites (≈160 kJ/mol) is compatible with the formation of H_2O/Lewis complexes within the nanocavities of the microporous system (see Figures 7 and 3, respectively).

3.5. Crystalline Microporous versus Amorphous Aluminosilicates. Comparison of H_2O adsorption data for crystalline microporous and amorphous alumino-silicate materials (H-zeolites and SA, respectively) might help in elucidating the nature and structure of acidic species originating from the presence of Al moieties in a silica matrix. For the sake of simplicity, only adsorption data for H−BEA zeolite will be compared with those for SA sample. It is known that a difference does exist in protonic acidity between zeolites and silico−alumina materials of similar composition.[42] In particular, Huang et al. have demonstrated that Brønsted acidic strength, strongly dependent on crystallinity degree of the material, is highest for H-zeolites.[9]

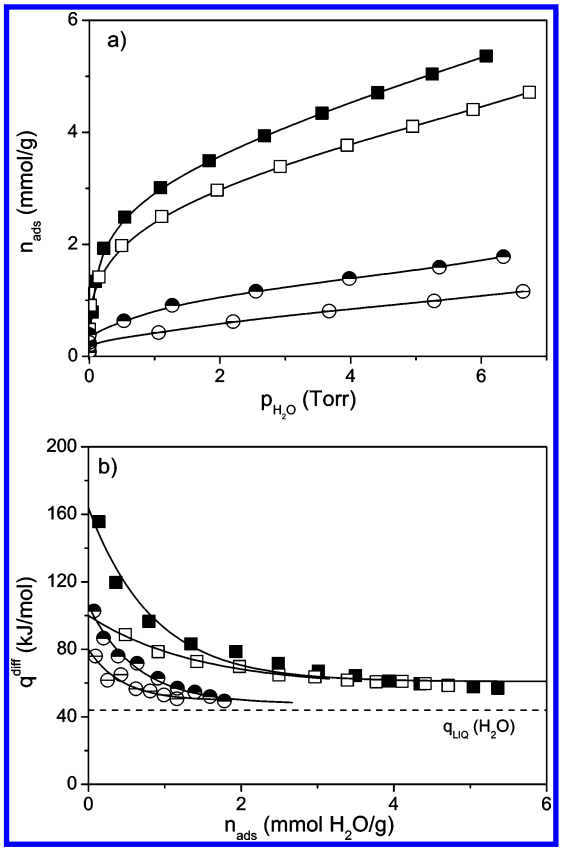

Figure 8. (a) Volumetric isotherms (adsorbed amounts vs equilibrium pressure) and (b) differential heats of adsorption (q^{diff} vs coverage) of H_2O adsorbed at 303 K on H−BEA (filled box, open box) and on SA, (half-filled circle, open circle with bisecting line). Solid symbols correspond to the first run; open symbols correspond to the second run.

In Figure 8, volumetric isotherms (part a) and differential heats of adsorption (part b) are reported for SA and H−BEA (calorimetric isotherms are omitted for the sake of brevity). Adsorbed amounts (n_{ads} mmol/g) for SA are now shown per gram of catalyst, to properly compare the amorphous SA and crystalline microporous H−BEA data. It is clearly evident (see also Table 1) that H−BEA is definitely more hydrophilic than SA: at $p = 5$ Torr H_2O uptake is 4.97 versus 1.53 mmol/g for H−BEA and SA, respectively. Integral molar heat of adsorption $[q^{mol}]_p$ developed at the same pressure (see Table 2) is only slightly higher for H−BEA (76 vs 67 kJ/mol for SA), whereas the irreversible component is dramatically larger for SA. The (ads I − ads II) component is indeed ≈40% of the total adsorption for SA and only ≈20% for H−BEA. This datum indicates that H_2O interaction with amorphous SA involves an irreversible modification of the surface much greater than for crystalline H−BEA.

To better understand the differences in H_2O adsorption mechanism, q^{diff} versus n_{ads} plots for SA and H−BEA are contrasted. By the inspection of Figure 8b, it appears that the energy of interaction of H_2O is dramatically higher for H−BEA than for amorphous SA, in the whole interval examined. At

vanishing coverage, q_0 is ~160 kJ/mol for H−BEA and only ~110 kJ/mol for SA. At high coverage, q^{diff} for the former lies well above $q_{LIQ} = 44$ kJ/mol, while for the latter it approaches q_{LIQ}. The same holds for the ads II reversible adsorption.

It is quite surprising that the high reactivity of SA toward H_2O, as witnessed by the large irreversible component, does involve a much lower energy of interaction than for H−BEA. A possible explanation is the following: in H-zeolite case, hydrophilic acidic sites belong to a rigid crystalline framework that does not allow severe surface reconstruction, at variance with what occurs at the surface of the more pliable amorphous Si−O−Al system. Reconstruction phenomena imply surface deformation processes, which are intrinsically endothermic and do contribute by an opposite sign to the heat of adsorption. Consequently, the measured heat is lower than what is expected for a plain adsorption, occurring on non-deformable sites. The same holds for both Brønsted and Lewis acidic sites. The latter in particular, by making part of a rigid zeolite framework, acquire a close similarity with Lewis sites exposed at transition alumina surface. Indeed, q^{diff} values for H_2O adsorbed on *cus* Al(III) sites in H-zeolites and in ALU are comparable (vide supra). By contrast, *cus* Al(III) species in SA are exposed at a Si−O−Al surface heavily reconstructed and are much less available for interacting with H_2O. This idea is supported also by modeling results on LC cluster (see Figure 2). The LC framework can be assumed as a model for amorphous SA, in which the Al atom is allowed to expand its coordination (so decreasing its Lewis character) as a consequence of Si−O−Si flexibility. When H_2O is adsorbed on such a Al(III) site, a fraction of the adsorption energy is lost to pull out the Al atom from its coordination with the framework. This process requires an energy cost amounting to some 25% of the total binding energy for the LCW case. The present results are in line with what was previously hypothesized by Busca and co-workers.[42]

4. Conclusions

The combined use of microcalorimetric and computational approaches has been adopted to describe the mechanism of H_2O interaction with the acidic sites located within the proton-exchanged zeolites nanocavities, of both Lewis and Brønsted nature. In particular, the enthalpy changes associated to the RT-adsorption of H_2O vapor have been determined by microcalorimetry for two Lewis-rich H-zeolites of different structure (H−BEA and a H−MFI) but are characterized by a very close silica-to-alumina ratio and an almost equal number of Al atoms per unit cell. The H_2O adsorption enthalpy has been determined also for all-silica zeolites, amorphous silica, and silico-alumina, transition alumina, chosen as experimental model systems. Adsorption experimental enthalpies have been compared to ab initio computed binding energies of H_2O interacting with model sites simulating (i) Lewis and Brønsted acidic sites (*cus* Al(III) and $Si(OH)^+Al^-$ species, respectively) and (ii) a variety of Si−OH species, either H-bonding interacting (nests and pairs) or isolated.

The first goal of the present work was to investigate the mechanism of water−zeolite interaction by analyzing and discussing various kinds of interactions a H_2O molecule can experience with specific (acidic) sites. The second goal was to better address the definition of the hydrophilic features of (acidic) zeolites, associated with polar species of various nature (*cus* Al(III), $Si(OH)^+Al^-$, Si−OH groups). The most significant results obtained are summarized in the following paragraphs.

(i) The interaction of H_2O with the H-zeolites acidic sites is dominated by the Al-site population, more than by the nanocavity topology or the acidic site nature. Both H−MFI and H−BEA, saturated with about 5 Torr of H_2O vapor, were found to bind ~4 H_2O molecules per Al site, almost one of which is tightly bound to the site, and is not eliminated by simple pumping-off at RT. For both H-zeolites, the experimental heats of adsorption were in the $160 < q^{diff} < 80$ kJ/mol interval for one H_2O molecule adsorbed per Al atom, on average. The second-to-fourth H_2O molecules were bound with an energy of interaction ($80 < q^{diff} < 60$ kJ/mol) larger than $q_L = 44$ kJ/mol.

(ii) Ab initio calculations have shown that the H_2O/Lewis site energy of interaction (160−109 kJ/mol range, according to the local coordination of Al(III) atom) is much larger than that of the H_2O/Brønsted site (65 kJ/mol). The zero-coverage heat of adsorption ($q_0 \approx 160$ kJ/mol, for both H-zeolites) has been thus assigned to the H_2O/Lewis complex formation, which dominates the early stage of the adsorption process.

(iii) The close similarity of the q^{diff} versus n_{ads} plots for the two H-zeolites has been interpreted to be due to similar distributions of Lewis and Brønsted sites, as well as to the simultaneous adsorption of H_2O on both kind of sites, without following an ordered path of site occupation based on the acidic strength. Further, as the experimental q^{diff} for the second-to-fourth H_2O shell formation is significantly larger than 44 kJ/mol, it has been inferred that the first shell H_2O molecules coordinated to Al(III) Lewis sites are strongly polarized, and possess an acidic strength which compares with the acidic strength of structural Brønsted sites. This was straightforwardly confirmed by ab initio calculations.

(iv) The simultaneous/competitive filling of Lewis and Brønsted sites upon H_2O adsorption did not allow us to straightforwardly assign a precise heat value for the H_2O/Brønsted complex formation, in that the first shell q^{diff} interval is comprehensive of the energy of both H_2O/Lewis and H_2O/Brønsted complexes formation. However, a 80−100 kJ/mol interval has been suggested as the most appropriate. This is in reasonable good agreement with present work calculated BEs and with data reported in the literature (both experimental heats and computational data).

(v) The all-silica zeolites investigated have been categorized as hydrophilic (opposite to what generally thought) in that they adsorb H_2O by forming adducts of relative stability, owing to the presence of defects (either Si−OH nests, or residual traces of Al species) in the hydrophobic Si−O−Si framework. Indeed, the measured heat of interaction of H_2O with such zeolites was found to be larger than $q_{LIQ} = 44$ kJ/mol. Modeling results, simulating the interaction of H_2O with surface hydroxyl groups in different topologies, support this interpretation.

(vi) Comparison between crystalline versus amorphous aluminosilicate heats of adsorption has shown, in line with modeling results, that a significant fraction of the adsorption energy is wasted to pull out the Al-containing acidic site from the amorphous matrix to bring it into an interaction with H_2O, at variance with the crystalline material in which acidic sites are already in place, as imposed by the rigidity of the framework.

Acknowledgment. This work was financially supported by Project PRISMA-INSTM 2002, coordinated by Prof. C. Morterra, University of Torino, Italy: "Nanostructured oxidic materials for the adsorption and the catalysis". P.U. is also indebted to Project MIUR-COFIN2004, Prot. 2004054901_003 coordinated by Prof. D. Ghigo University of Torino, Italy. Dr. G. Spanò and F. Rivetti (Polimeri Europa srl. Centro Ricerche Novara Istituto G. Donegani Novara, Italy) are greatly acknowl-

edged for kindly supplying the microporous samples (H−BEA, H−MFI, MFI−Silicalite) studied in the present work. Prof. L. Forni and Dr. M. Bregolato, University of Milano, Italy, are greatly acknowledged for especially preparing the all-silica BEA−Silicalite specimen.

References and Notes

(1) Corma, A. *Chem. Rev.* **1995**, *95*, 559.
(2) Farneth, W. E.; Gorte, R. J. *Chem. Rev.* **1995**, *95*, 615.
(3) Auroux, A. *Top. Catal.* **2002**, *19*, 205.
(4) Zecchina, A.; Otero Areán, C. *Chem. Soc. Rev.* **1996**, 187.
(5) Zecchina, A.; Lamberti, C.; Bordiga, S. *Catal. Today* **1998**, *41*, 169.
(6) Gorte, R. J. *Catal. Lett.* **1999**, *62*, 1.
(7) Garrone, E.; Rodriguez Delgado, M.; Otero Arean, C. *Trends Inorg. Chem.* **2001**, *7*, 119.
(8) Parrillo, D. J.; Lee, C.; Gorte, R. J.; White, D.; Farneth, W. E. *J. Phys. Chem.* **1995**, *99*, 8745.
(9) Huang, M.; Auroux, A.; Kaliaguine, S. *Microporous Mater.* **1995**, *5*, 17.
(10) Narayanan, S.; Sultana, A.; Le, Q. T.; Auroux, A. *Appl. Catal., A.* **1998**, *168*, 373.
(11) Savitz, S.; Meyers, A. L.; Gorte, R. J.; White, D. *J. Am. Chem. Soc.* **1998**, *120*, 5701.
(12) Savitz, S.; Meyers, A. L.; Gorte, R. J.; White, D. *Microporous Mesoporous Mater.* **1999**, *31*, 211.
(13) Auroux, A. *Top. Catal.* **1997**, *4*, 71.
(14) Blumenfeld, A. L.; Fripiat, J. J. *Top. Catal.* **1997**, *4*, 119.
(15) Arean, C. O.; Palomino, G. T.; Platero, E. E.; Mentruit, M. P. *J. Chem. Soc., Dalton Trans.* **1997**, 873.
(16) Kunkeler, P. J.; Zuurdeeg, B. J.; Waal, J. C. v. d.; Bockoven, J. A. v.; Koningsberger, D. C.; Bekkum, H. v. *J. Catal.* **1998**, *180*, 234.
(17) Pazè, C.; Bordiga, S.; Lamberti, C.; Salvalaggio, M.; Zecchina, A.; Bellussi, G. *J. Phys. Chem. B* **1997**, *101*, 4740.
(18) Jacobs, P. A.; Beyer, H. K. *J. Phys. Chem. B* **1979**, *83*, 1174.
(19) Pöppl, A.; Rudolf, T.; Michel, D. *J. Am. Chem. Soc.* **1998**, *120*, 4879.
(20) Remy, M. J.; Stanica, D.; Poncelet, G.; Feijen, E. J. P.; Grobet, P. J.; Martens, J. A.; Jacobs, P. A. *J. Phys. Chem.* **1996**, *100*, 12440.
(21) Shannon, R. D.; Gardner, K. H.; Staley, R. H.; Bergeret, G.; Gallezot, P.; Auroux, A. *J. Phys. Chem.* **1985**, *89*, 4778.
(22) Jansen, J. C.; Creyghton, E. J.; Njo, S. L.; Koningsveld, H. v.; Bekkum, H. v. *Catal. Today* **1997**, *38*, 205.
(23) Jia, C.; Massani, P.; Barthomeuf, D. *J. Chem. Soc., Faraday Trans.* **1993**, *89*, 3659.
(24) Bolis, V.; Broyer, M.; Barbaglia, A.; Busco, C.; Foddanu, G. M.; Ugliengo, P. *J. Mol. Catal. A: Chem.* **2003**, *204*, 561.
(25) Bolis, V.; Barbaglia, A.; Broyer, M.; Busco, C.; Civalleri, B.; Ugliengo, P. *Origins Life Evol. Biosphere* **2004**, *34*, 69.
(26) Busco, C.; Barbaglia, A.; Broyer, M.; Bolis, V.; Foddanu, G. M.; Ugliengo, P. *Thermochim. Acta* **2004**, *418*, 3.
(27) Bolis, V.; Busco, C.; Bordiga, S.; Ugliengo, P.; Lamberti, C.; Zecchina, A. *Appl. Surf. Sci.* **2002**, *196*, 56.
(28) Bordiga, S.; Roggero, I.; Ugliengo, P.; Zecchina, A.; Bolis, V.; Artioli, G.; Buzzoni, R.; Marra, G. L.; Rivetti, F.; Spanò, G.; Lamberti, C. *J. Chem. Soc., Dalton Trans.* **2000**, 3921.
(29) Busca, G. *Catal. Today* **1998**, *41*, 191.
(30) Bevilacqua, M.; Alejandre, A. G.; Resini, C.; Casagrande, M.; Ramirez, J.; Busca, G. *Phys. Chem. Chem. Phys.* **2002**, *4*, 4575−4583.
(31) Bevilacqua, M.; Busca, G. *Catal. Commun.* **2002**, *3*, 497.
(32) Gorte, R. J.; White, D. *Microporous Mesoporous Mater.* **2000**, *35*−*36*, 447.
(33) Derouane, E. G.; Chang, C. D. *Microporous Mesoporous Mater.* **2000**, *35*−*36*, 425.
(34) Yang, L.; Trafford, K.; Kresnawahjuesa, O.; Sepa, J.; Gorte, R. J.; White, D. *J. Phys. Chem. B* **2001**, *105*, 1935.
(35) Bregolato, M.; Bolis, V.; Busco, C.; Bordiga, S.; Cavani, F.; Ugliengo, P.; Forni, L. *J. Catal.*, in preparation.
(36) Davydov, V. Y. In *Adsorption on Silica Surfaces*; Papirer, E., Ed.; Marcel Dekker: New York, 2000; Vol. 4, p 63.
(37) Morrow, B. A.; Gay, I. D. Infrared and NMR Characterization of the Silica Surface. In *Adsorption on Silica Surfaces*; Papirer, E., Ed.; Marcel Dekker: New York, 2000; Vol. 2, p 9.
(38) Zhuralev, L. T. *Colloids Surf., A* **2000**, *173*, 1.
(39) Della Gatta, G.; Fubini, B.; Strabella, L. *J. Chem. Soc., Faraday Trans. 2* **1977**, *73*, 1040.
(40) Morterra, C.; Magnacca, G. *Catal. Today* **1996**, *27*, 497.
(41) Bolis, V.; Cerrato, G.; Magnacca, G.; Morterra, C. *Thermochim. Acta* **1998**, *312*, 63.
(42) Trombetta, M.; Busca, G.; Rossini, S.; Piccoli, V.; Cornaro, U.; Guercio, A.; Catani, R.; Willey, R. J. *J. Catal.* **1998**, *179*, 581.
(43) Cardona-Martinez, N.; Dumesic, J. A. *J. Catal.* **1990**, *125*, 427.
(44) Bolis, V.; Barbaglia, A.; Bordiga, S.; Lamberti, C.; Zecchina, A. *J. Phys. Chem. B* **2004**, *108*, 9970.
(45) Bolis, V.; Maggiorini, S.; Meda, L.; D'Acapito, F.; Palomino, G. T.; Bordiga, S.; Lamberti, C. *J. Chem. Phys.* **2000**, *113*, 9248.
(46) Parrillo, D. J.; Gorte, R. J. *J. Phys. Chem.* **1993**, *97*, 8786.
(47) Cardona-Martinez, N.; Dumesic, J. *Adv. Catal.* **1992**, *38*, 149.
(48) Gravelle, P. C. *Adv. Catal.* **1972**, *22*, 191.
(49) Fubini, B.; Bolis, V.; Bailes, M.; Stone, F. S. *Solid State Ionics* **1989**, *32*−*33*, 258.
(50) Bolis, V.; Fubini, B.; Marchese, L.; Martra, G.; Costa, D. *J. Chem. Soc., Faraday Trans.* **1991**, *87*, 497.
(51) Auroux, A. In *Catalyst Characterization: Physical Techniques for Solid Materials*; Imelik, B., Vedrine, J. C., Eds.; Plenum Press: New York, 1994; Vol. 22, p 611.
(52) Bolis, V.; Cavenago, A.; Fubini, B. *Langmuir* **1997**, *13*, 895.
(53) Cerruti, M.; Bolis, V.; Magnacca, G.; Morterra, C. *Phys. Chem. Chem. Phys.* **2004**, *6*, 2468.
(54) Civalleri, B.; Casassa, S.; Garrone, E.; Pisani, C.; Ugliengo, P. *J. Phys. Chem. B* **1999**, *103*, 2165.
(55) Civalleri, B.; Ugliengo, P. *J. Phys. Chem. B* **2000**, *104*, 9491.
(56) Boys, S. F.; Bernardi, F. *Mol. Phys.* **1970**, 553.
(57) Heitmann, G. P.; Dahlhoff, G.; Hölderich, W. F. *J. Catal.* **1999**, *186*, 12.
(58) Narayanan, S.; Sultana, A.; Meriaudeau, P.; Naccache, C.; Auroux, A.; Viornery, C. *Appl. Catal., A* **1996**, *143*, 337.
(59) Armaroli, T.; Trombetta, M.; Gutierrez Alejandre, A.; Ramirez Solis, J.; Busca, G. *Phys. Chem. Chem. Phys.* **2000**, *2*, 3341.
(60) Sauer, J.; Ugliengo, P.; Garrone, E.; Saunders, V. R. *Chem. Rev.* **1994**, *94*, 2095.
(61) Tuma, C.; Sauer, J. *Chem. Phys. Lett.* **2004**, *387*, 388.
(62) Ison, A.; Gorte, R. J. *J. Catal.* **1984**, *89*, 150.
(63) Olson, D. H.; Zygmunt, S. A.; Erhardt, M. K.; Curtiss, L. A.; Iton, L. E. *Zeolites* **1997**, *18*, 347.
(64) Lee, C.-C.; Gorte, R. J.; Farneth, W. E. *J. Phys. Chem. B* **1997**, *101*, 3811.
(65) Olson, D. H.; Haag, W. O.; Borghard, W. S. *Microporous Mesoporous Mater.* **2000**, *35*−*36*, 435.
(66) Fubini, B. *Thermochim. Acta* **1988**, *135*, 19.
(67) Zettlemoyer, A. C.; Micale, F. J.; Klier, K. In *Water: A Comprehensive Treatise*; Franks, F., Ed.; Plenum Press: New York, 1975; Vol. 5, p 249.
(68) Ugliengo, P.; Saunders, V.; Garrone, E. *J. Phys. Chem.* **1990**, *94*, 2260.
(69) Civalleri, B.; Garrone, E.; Ugliengo, P. *J. Phys. Chem. B* **1998**, *102*, 2373.
(70) Civalleri, B.; Garrone, E.; Ugliengo, P. *Chem. Phys. Lett.* **1999**, *299*, 443.
(71) Fubini, B.; Bolis, V.; Cavenago, A.; Ugliengo, P. *J. Chem. Soc., Faraday Trans.* **1992**, *88*, 277.